Magnetic Field Sensor Based on Directional Coupling in a Magnetic Fluid-Filled Photonic Crystal Fiber

Yingchao Liu , Lijun Zhang , Shuang Ren , Rundong Zhang * , Peigang Cao * , Hailiang Chen *

Posted Date: 26 July 2023

doi: 10.20944/preprints202307.1726.v1

Keywords: magnetic field sensor; photonic crystal fiber; magnetic fluid; modes coupling

Article

Magnetic Field Sensor Based on Directional Coupling in a Magnetic Fluid-Filled Photonic Crystal Fiber

Yingchao Liu [1,‡], Lijun Zhang [1,‡], Shuang Ren [1], Rundong Zhang [1,*], Peigang Cao [2,*] and Hailiang Chen [3,*]

[1] Key Laboratory of Industrial Intelligent Perception, School of artificial Intelligence, North China University of Science and Technology, Tangshan 063210, China
[2] Tangshan Caofeidian Industrial Port Co., LTD, Tangshan 063210, China
[3] State Key Laboratory of Metastable Materials Science & Technology and Key Laboratory for Microstructural Material Physics of Hebei Province, School of Science, Yanshan University, Qinhuangdao 066004, China
* Correspondence: rung_bj2008@163.com; gpcsygs@163.com; hlchen@ysu.edu.cn
‡ These authors contributed equally to this work.

Abstract: In this paper, a sensitivity sensor of dual-core photonic crystal fiber (DC-PCF) filled with magnetic liquid is introduced and investigated by the finite element method (FEM). To regulate the energy coupling involving the two cores, the magnetic fluid is filled into the pore between the two cores. To adjust the coupling between the supermodes in the DC-PCF, the refractive index of the magnetic fluid-filled air hole may change due to the external magnetic field. This specifically created a magnetic fluid-filled DC-PCF, the magnetic fluid-filled hole is not used as the core for energy transmission, thus avoiding transmission loss. The dip wavelength and the magnetic field displayed an excellent linear connection between 80 and 260 Oe, depending on the numerical data. The detection sensitivity of the magnetic field reached 515.75 pm/Oe at a short fiber length of 482 μm. The designed magnetic fluid-filled DC-PCF has high sensitivity and small volume and has great application prospects in medical and industrial field magnetic field detection.

Keywords: magnetic field sensor; photonic crystal fiber; magnetic fluid; modes coupling

1. Introduction

Magnetic fluid (MF), also known as ferromagnetic fluid, is a new type of functional material. It has not only the fluidity of liquid, but also the magnetism of solid magnetic material. MF is a stable colloidal liquid which is composed of magnetic nanoparticles, liquid carriers, and surfactant[1]. The magnetic nanoparticles can be prepared by chemical coprecipitation[2]. The magnetic nanoparticles surrounded by surfactants are evenly dispersed in the liquid carriers. The refractive index of MF depicts a linear relationship with the concentration of magnetic nanoparticles. As the external magnetic field intensity is higher than a critical value, the relationship between the refractive index of MF and magnetic field complies the Langevin equation[3]. Owing to the magneto-optical characteristics of MF, many optical devices such as wavelength filters, optical switches and magnetic field sensors have been proposed[4–7]. Photonic crystal fiber (PCF), also known as microstructured optical fiber or holey fiber, was firstly fabricated by Knight, J. C. et al. in 1996[8]. Moutusi De et al. designed a magnetic field sensor with a sensitivity of 799.07 pm/Oe using square lattice PCF[9]. Li et al. designed a sensor for magnetic fields built on an MF-filled DC-PCF. The two MF-filled air holes serve as two separate waveguides. The sensitivity was 4.8 pm/Oe based on the modes coupling effect[10]. Liu et al. investigated a PCF Sagnac interferometer filled with MF and found that it had an average sensitivity of 384 pm/Oe between 410 and 600 Oe[11]. Xu et al. designed a novel PCF magnetic field sensor with two elliptic center holes filled with magnetic fluid and some elliptic cladding air holes. The sensitivity of the magnetic sensor was calculated. The numerical simulation results showed that the maximum sensitivity of the magnetic sensor could reach 1200 pm/Oe[12]. However, according to the previously reported DC-PCF magnetic field sensors, the structure of PCF was usually complex.

Preprints (www.preprints.org) | NOT PEER-REVIEWED | Posted: 26 July 2023 doi:10.20944/preprints202307.1726.v1

Even in some PCFs, light is transmitted in the high loss magnetic fluid. It is essential to investigate a DC-PCF magnetic field sensor with high sensitivity and vitally light transmission in silica core.

In this paper, a magnetic field sensor based on a MF-filled DC-PCF was investigated using the finite element method. Only one central air hole in the DC-PCF was designed to be infiltrated with MF. The mode coupling effect between the supermodes could be adjusted by the external magnetic field. Numerical results showed that the measuring sensitivity reached 515.75 pm/Oe. The wavelength shift showed a linear relationship with the magnetic field intensity in the range of 80-260 Oe, which made it a significant candidate in the measurement of magnetic field.

2. MF-Filled DC-PCF and Operation Principle

As seen in Figure 1(a), the cross-section of the MF-filled DC-PCF. The air holes are arranged in a rectangular lattice. Compared with hexagonal distribution, rectangular arrangement of holes can generate greater mode birefringence[13]. Depicting larger mode birefringence leads to shorter coupling lengths. Thus, the size of the DC-PCF magnetic field sensor can be made much smaller. The spacing of surrounding voids are indicated by Λ_x in the horizontal direction and Λ_y in the vertical direction, respectively. Both the values of Λ_x and Λ_y are set at 2 μm. The corresponding values of d_1, d_2, and d_3 represent the diameters of the tiny white, huge white, and small black air holes, respectively. These diameters are initially set at d_1 = 1.2 μm, d_2 = 1.6 μm, and d_3 = 1.2 μm, respectively. It is well known that the efficient refractive indices of core modes are mainly influenced by its most adjacent air holes[14]. To achieve magnetic field detection, the center air hole is fashioned as an MF infiltration hole. The filling technology demonstrated by[15,16], can be used to achieve the selective infilling of MF. Figure 1(b) depicts the meshed cross-section of the DC-PCF. Perfectly Matched Layer (PML) is used to absorb the energy of the scattering light. The scattering boundary condition (SBC) acts as the PML's outer boundary to further enhance the absorption of scattering light. The COMSOL Multiphysics software meshes the computational region using free triangles. The DC-PCF is meshed into about 16814 elements. In the designed DC-PCF, the refractive index of air is set as n_{air} = 1. Fused silica glass serves as the back ground material of DC-PCF, and the Sellmeier equation can be used to determine its material dispersion[17].

$$n^2(\lambda) = 1 + \frac{m_1\lambda^2}{\lambda^2 - {k_1}^2} + \frac{m_2\lambda^2}{\lambda^2 - {k_\lambda}^2} + \frac{m_3\lambda^2}{\lambda^2 - {k_3}^2} \tag{1}$$

where λ is the wavelength in free space and its unit is μm. The parameters in equation (1) are m_1 = 0.6961663, m_2 = 0.4079426, m_3 = 0.8974794, k_1 = 0.0684043 μm, k_2 = 0.1162414 μm, and k_3 = 9.896161 μm. The Langevin function is followed by the refractive index of MF[18].

$$n(H,T) = [n_t - n_i]\left[\coth\left(\alpha\frac{H - H_{i,n}}{T}\right) - \frac{T}{\alpha\,(H - H_{i,n})}\right] + n_t, (H > H_{i,n}) \tag{2}$$

where n(H, T) is the refractive index of the MF fluctuation with temperature and magnetic field strength, n_t is the refractive index value as MF reaches the saturation magnetization, and the magnetic field's threshold value is $H_{i,n}$. The refractive index of MF is n_i because the magnetic field H is smaller than $H_{i,n}$. The temperature in Kelvin is T. α denotes the coefficient of the fitting.

In this paper, MF is carried by water as its liquid carrier, and its concentration is 25%. The parameters are $H_{i,n}$ = 80 Oe, n_i = 1.3411, n_t = 1.3901, α = 0.143, and T = 293 K[18]. In Figure 2, the refractive index of the MF fluctuation is shown along with the magnetic field strength H.

The block diagram of the suggested sensor based on an MF-filled DC-PCF is shown in Figure 3. The MF-filled DC-PCF is spliced with two single mode fibers (SMFs). A broadband source (BBS) provides continuous light. The incident light is launched into the left SMF. Then, it passes through the MF-filled DC-PCF and enters the right SMF. It eventually arrives at the optical spectrum analyzer (OSA). The DC-PCF filled with MF is given a magnetic field by the solenoid, which is then used to modify the MF's refractive index.

Preprints (www.preprints.org) | NOT PEER-REVIEWED | Posted: 26 July 2023 doi:10.20944/preprints202307.1726.v1

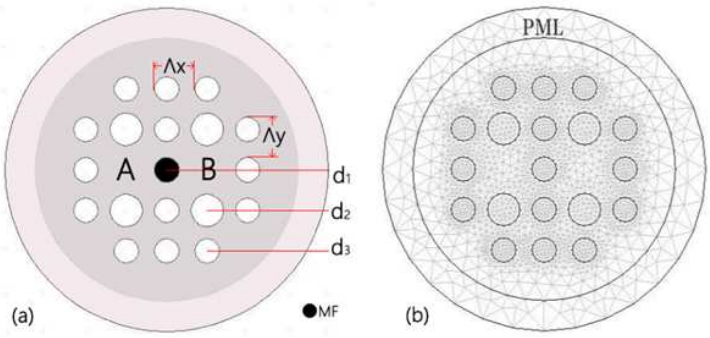

Figure 1. (a) Cross section of the MF-filled DC-PCF. (b) FEM mesh and PML.

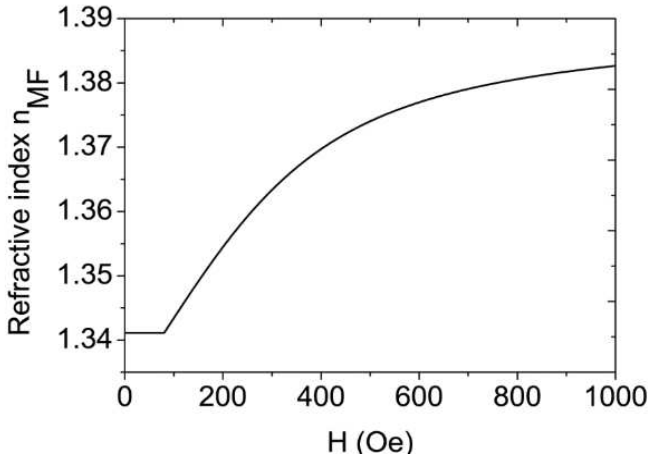

Figure 2. The refractive index of MF variation with magnetic field.

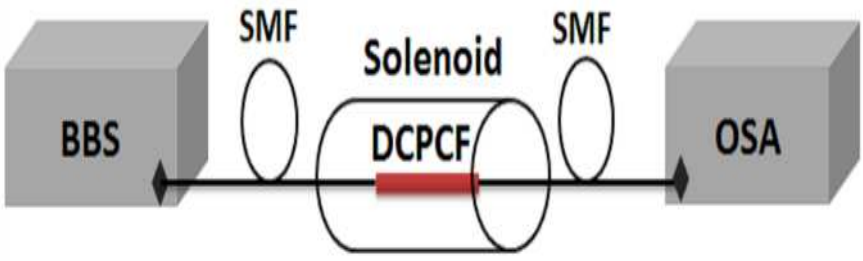

Figure 3. MF-filled DC-PCF-based magnetic field sensor schematic diagram.

The two silica cores besides the central MF-filled hole in DC-PCF form two independent waveguides. According to the supermodes theory, there are four supermodes, comprising x-polarized even mode, x-polarized odd mode, y-polarized even mode, and so on. The model properties of the four supermodes are calculated using COMSOL Multiphysics software. Figure 4 displays the electrical field distributions at 1.55 μm wavelength.

Preprints (www.preprints.org) | NOT PEER-REVIEWED | Posted: 26 July 2023 doi:10.20944/preprints202307.1726.v1

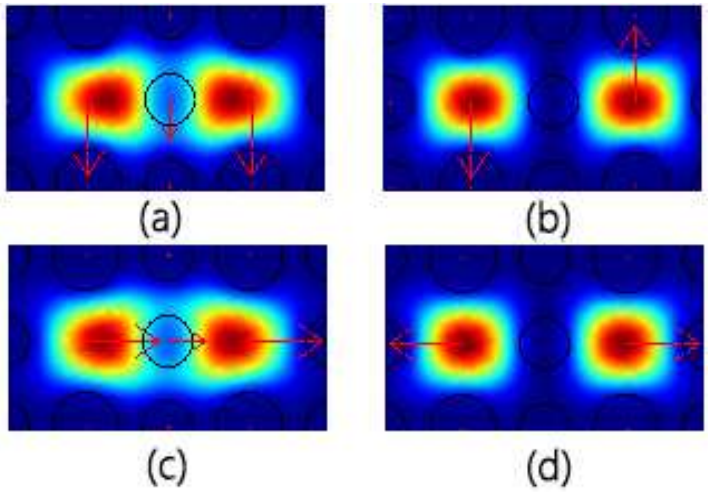

Figure 4. Electric filed distributions of the four supermodes. (a)even mode with a polarization of y, (b) odd mode with a polarization of y, (c) even mode with a polarization of x, and (d) odd mode with a polarization of x.

The coupling length (L_i) between the supermodes can be described as[19].

$$L_i = \frac{\pi}{\left|\beta_e^i - \beta_o^i\right|} = \frac{\pi}{2\left|n_e^i - n_o^i\right|}, i = x, y \tag{3}$$

where β_e^i , β_o^i are the propagation constants and n_e^i , n_o^i are the actual refractive indices. The even and odd supermodes are represented by e and o, respectively. I represents the polarized direction. The parameters are set as d_1 = 1.2 μm, d_2 = 1.6 μm, d_3 = 1.2 μm, $\Lambda_x = \Lambda_y$ = 2 μm, and H = 80 Oe. At a wavelength of 1.55 μm, the simulated actual refractive indices of the four foudamental are n_e^x =1.4110976, n_o^x = 1.406277541, n_e^y = 1.409642134, and n_o^y = 1.404987619. The coupling distances calculated by Eq. (3) are 160.8 μm and 166.5 μm for the two polarized directions that are orthogonal. Coupling length is a vital parameter for DC-PCF. Power can flow from one core to the other at the coupling length. It is thought that the light is fired at the input ports of cores A. The normalized power in the input ports of cores A and B is set at 1 and 0, respectively[20]. You can define the normalized power at the output port of A as[21].

$$NP_i = \frac{P_{i-\,\mathrm{out}}}{P_{\mathrm{in}}} = \cos^2\left(\frac{\pi L}{2L_i}\right), i = x, y \tag{4}$$

where NP_i is the normalized output power. P_{in} =1 and $P_{i-\,\mathrm{out}}$ are the power of incident light and output light at core A, respectively. L denotes the length of MF-filled DC-PCF. It is possible to compute the output power in dB:

$$T_i = 10\log_{10}\left(NP_i\right), \quad i = x, y \tag{5}$$

The transmission spectrum fluctuates as a result of variations in supermode refractive indices and magnetic field changes. Using the directional coupling principle, the magnetic field can be found by monitoring the dip wavelength. The sensitivity S(H) can be calculated by the following equation.

$$S(H) = \frac{\Delta\lambda_{\mathrm{dip}}}{\Delta H} \tag{6}$$

where $\Delta\lambda_{\mathrm{dip}}$ is the shift of dip wavelength and ΔH is the variation of magnetic field intensity.

Preprints (www.preprints.org) | NOT PEER-REVIEWED | Posted: 26 July 2023 doi:10.20944/preprints202307.1726.v1

3. Results and Discussion

According to Eq. (3), it is determined that there is a wavelength link between supermode coupling length and refractive index. Figure 5(a) and Figure 5(b) depict, respectively, how coupling length and refractive index difference change with wavelength. At 80 Oe, the magnetic field's strength is determined. The discrepancy in Δn_{eo}'s refractive index grows as wavelength increases. The coupling lengths thus shorten in both orthogonal directions. Moreover, the coupling length in the y-polarization direction is more significant than in the x-polarization direction.

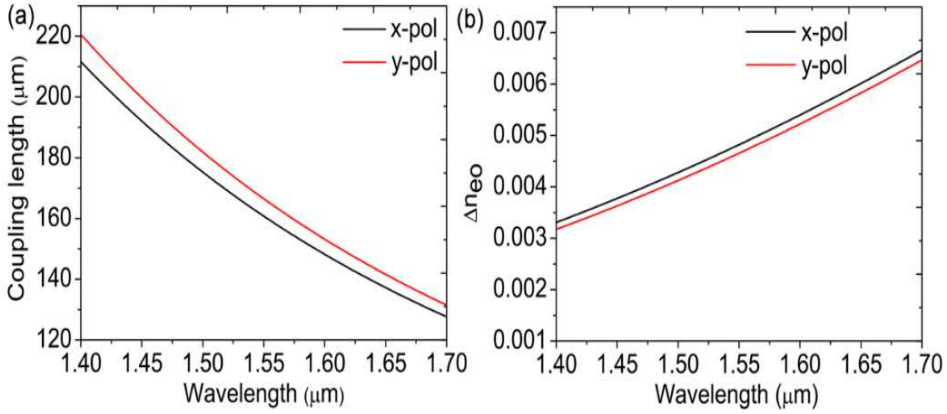

Figure 5. (a) Coupling length and as a function of wavelength, (b)the difference in the refractive indices of supermodes. The magnetic field is set at 80 Oe.

According to Eqs. (4) and (5), the transmission spectrum is correlated with both the DC-PCF length and coupling length. Since 1.55 μm is usually the communication wavelength, many devices are designed at 1.55 μm. Moreover, we use 1.55 μm as the reference wavelength. Figure 6 displays the transmission spectrum in the x-polarized direction. The DC-PCF length and magnetic field are set as 482 μm and 80 Oe. A visual trough is formed at the 1.55 μm communication window. Then, the magnetic field sensing characteristics of the DC-PCF are analyzed theoretically.

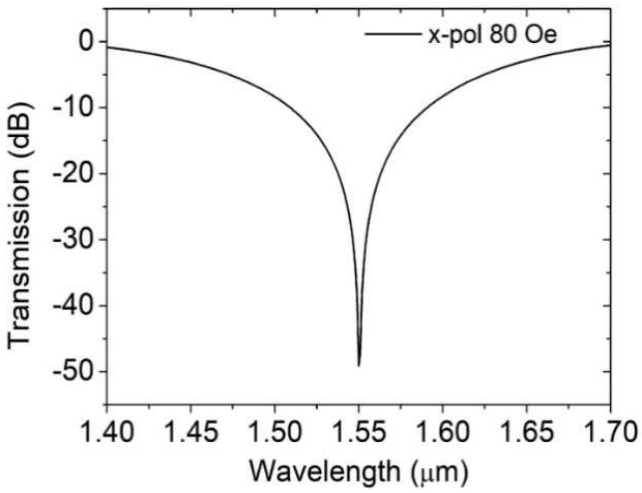

Figure 6. Transmission spectrum in x-polarized direction. The DC-PCF length and magnetic field are 482 μm and 80 Oe, respectively.

As the magnetic field intensifies, the refractive index of the MF rises. The refractive indices of the supermodes differ correspondingly. Figure 7(b) shows variations in dip wavelength shift with the magnetic field and Figure 7(a) transmission spectra at various magnetic field intensities. The dip wavelength moves toward the blue end of the spectrum from 80 to 260 Oe of magnetic field strength.

Preprints (www.preprints.org) | NOT PEER-REVIEWED | Posted: 26 July 2023 doi:10.20944/preprints202307.1726.v1

Because of this, the coupling wavelength is sensitive to variations in the strength of the magnetic field, and the strength of the external magnetic field can be estimated by measuring the coupling wavelength in the transmission spectrum.

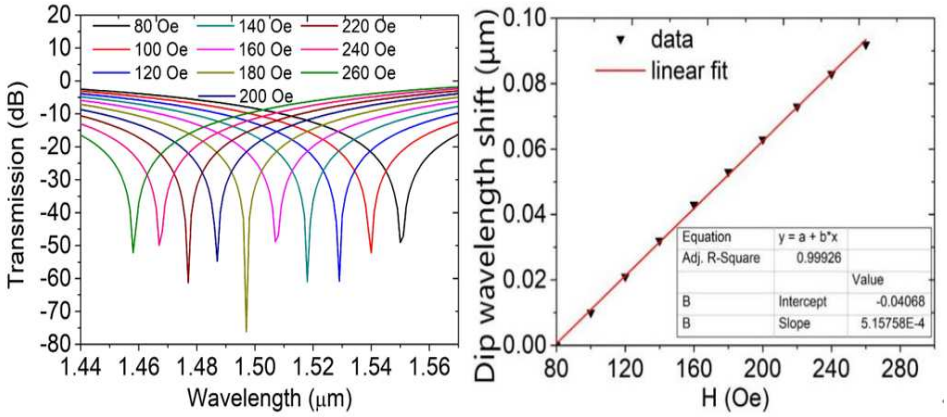

Figure 7. (a) Transmission spectra at different intensities of the magnetic field and (b) Dip wavelength shift variation with the magnetic field.

As seen in Figure 7(b), there is a linear relationship between the coupling wavelength and the strength of the magnetic field. The relation curve of the two is fitted, and the slope and fitting variance can be obtained. The physical meaning of the slope is the DC-PCF magnetic field sensor's sensitivity, and the sensor's sensitivity is 515.75 pm/Oe. The magnetic field strength and the coupling wavelength exhibit a strong linear relationship, as shown by the fitting variance of 0.99926. It offers many benefits and lowers the measuring error of magnetic fields as a magnetic field sensor. We generated and examined the transmission spectra at various structural parameters to investigate the impact of the PCF's structural factors on magnetic field detection performance.

Figure 8 shows the variation in the shift of dip wavelength with the magnetic field at different diameters d_1. The DC-PCF length has been adjusted at L=482 μm. When d_1 increases, the discrepancy between the effective refractive indices of the four supermodes and those indices also decreases. The coupling length lengthens as d_1 rises. The slopes of the curves determine the sensitivity of the magnetic field intensity sensor. The simulation results demonstrate that the magnetic field intensity sensor's sensitivity increases as diameter d_1 grows. The sensitivity of the magnetic field sensor is 500, 515.75, and 522.72 pm/Oe as d_1 is 1.16, 1.20, and 1.24 μm, respectively, as can be seen by comparing Figure 7(b) and Figure 8. As d_1 rises, the sensitivity rises as well. An increase in coupling length enhances the interaction between the transmitted light in the fiber cores and the magnetic fluid, increasing sensitivity.

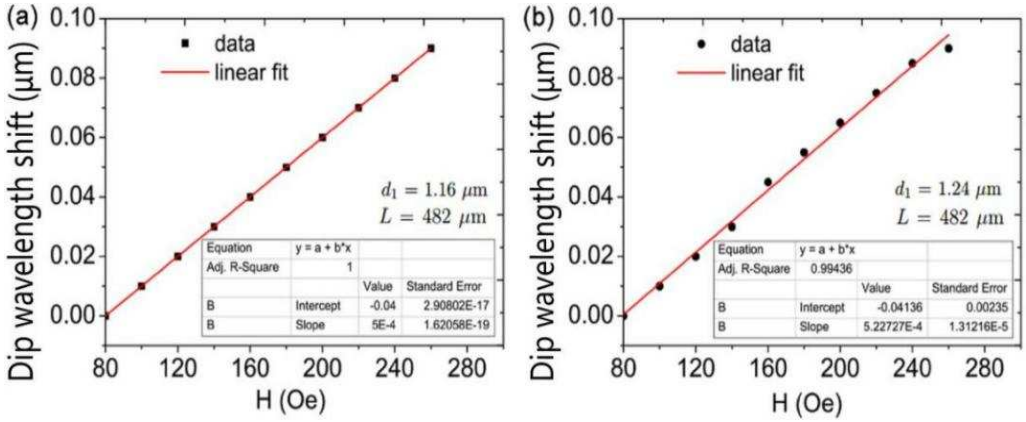

Figure 8. Dip wavelength shift varying with magnetic field intensity at (a) d_1= 1.16 μm and (b) d_1= 1.24 μm. L = 482 μm.

Preprints (www.preprints.org) | NOT PEER-REVIEWED | Posted: 26 July 2023 doi:10.20944/preprints202307.1726.v1

Dip wavelength shift varying with magnetic field intensity at different diameters d_2 is shown in Figure 9. DC-PCF length is set as L= 482 μm. The difference between the effective refractive indices of the supermodes increases as the effective refractive indices of the four supermodes decrease as d_2 increases. As a result, the coupling length shortens with increasing d_2, and a blue shift in the wave trough is seen. The sensitivity of the DC-PCF sensor greatly rises as the diameter d_2 rises from 1.56 to 1.64 μm, as can be shown in Figures 9 and 7(b). The sensitivity is 504.54, 515.75, and 531.81 pm/Oe for d_2=1.56, 1.60, and 1.64 μm, respectively. The transmitted light in the core is first compressed as d_2 rises, enhancing the sensitivity and mode coupling strength.

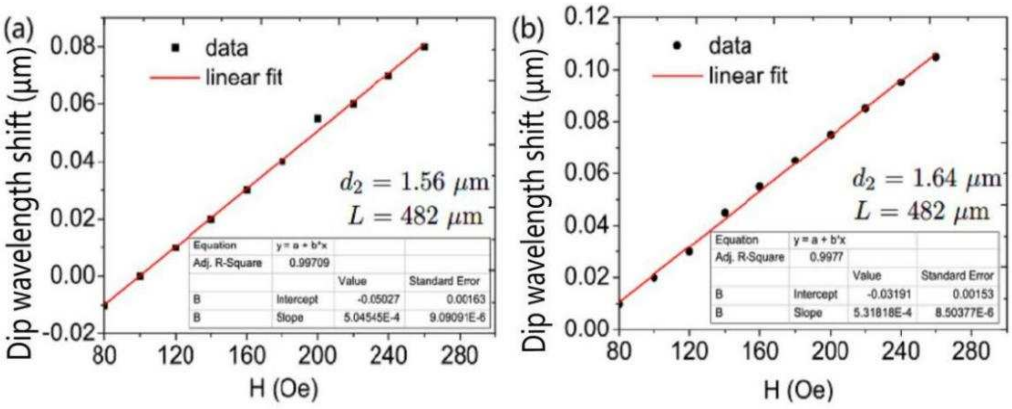

Figure 9. Dip wavelength shift varying with magnetic field intensity at (a) d_2 = 1.56 μm and (b) d_2 = 1.64 μm. L = 482 μm.

The dip wavelength shift is shown in Figure 10 as a function of the magnetic field strength at various d_3 diameters. The length of the DC-PCF is fixed to L = 482 μm. As d_3 is the hole that magnetic fluid fills, as d_3 increases, so does the magnetic fluid region. When d_3 increases, there is a decreasing disparity between the effective refractive indices of the four supermodes and their combined effective refractive indices. The coupling length lengthens as a result, the wave trough undergoes a red shift, and the sensitivity is improved. As d_3 = 1.24 μm, the sensitivity increases to 524.24 pm/Oe.

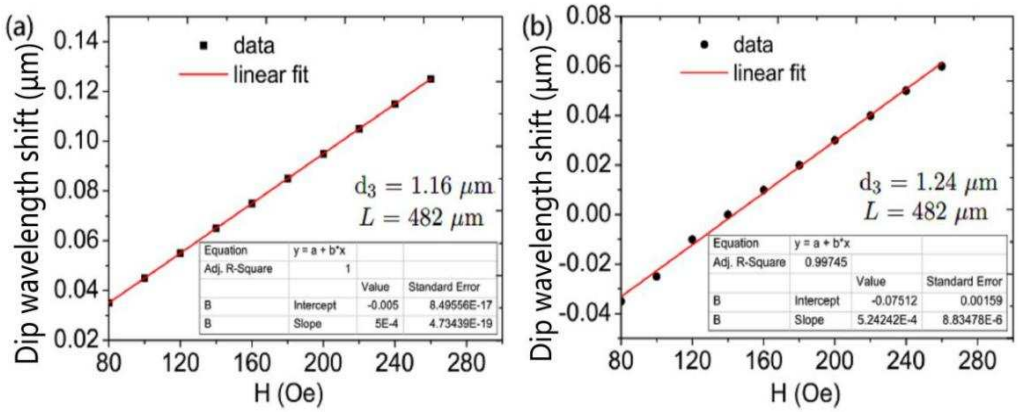

Figure 10. Dip wavelength shift varying with magnetic field intensity at (a) d_3 = 1.16 μm and (b) d_3 = 1.24 μm. L = 482 μm.

Table 1 shows the comparison of MF and fiber-based magnetic field sensors. Many sensor types, such as birefringence interference [22], Mach-Zehnder interference [23,25,26], Fabry-Perot interference [24], Sagnac interference [27,28], surface plasmon resonance [28], and directional coupling [10], have been used to detect the magnetic field. Some of the magnetic field sensors [24,27]did not have a linear responses which reduces the accuracy of the sensor and limits their applications. Due to the strong absorption of light by magnetic fluid, the optical signal will be feeble when light reflects from or passes

 doi:10.20944/preprints202307.1726.v1

through the magnetic fluid [10,23]. Our proposed magnetic field sensor used the directed coupling in MF-filled DC-PCF. A linear response of 80-260 Oe was used to attain the high sensitivity of 524.2 pm/Oe.

Table 1. Comparison of magnetic field sensors based on MF-filled optica

Sensor Type and Reference	Detection Range (Oe)	Linear Fitting	Sensitivity (pm/Oe)
Birefringence Interference[22]	0-450	Yes	24.2
SMF-PCF-SMF[23]	0-450	Yes	24.2
Fabry-Perot interference[24]	0-450	Yes	24.2
SMF-No Core Fiber-SMF[25]	40-100	Yes	90.5
Tapered and Lateral Spliced SMFs[26]	38-225	Yes	14.1
	250-475	Yes	26
Directional Coupling[10]	0-300	Yes	4.8
Sagnac interference [27]	0-2000	No	4.8(Maximum)
Sagnac interference [11]	410-600	Yes	384
Surface Plasmon Resonance[28]	0-500	Yes	44
Directional Coupling (This work)	80-260	Yes	524.24

4. Conclusions

A unique magnetic field sensor based on the DC-PCF has been developed using the finite element method. The shift in the wavelength of the dip can be used to calculate the external magnetic field. The simulated results show a strong linear link between the magnetic field in the 80-260 Oe region and the inclination wavelength shift. The highest level of sensitivity is 531.81 pm/Oe. Meanwhile, the magnetic sensing performance can be further improved by optimizing the DC-PCF structural parameters. Our MF-filled DC-PCF can successfully reduces the loss caused by magnetic fluid, showing a good prospect of magnetic field sensing.

Author Contributions: Conceptualization, Y.L., L.Z., and S.R.; writing—original draft preparation, Y.C., R.Z., P.C., L.Z., H.C.; and writing—review and editing, Y.L., H.C., L.Z., R.Z, P.C.and S.R.; All authors have read and agreed to the published version of the manuscript.

Funding: This research was funded by National Natural Science Foundation of China grant number 12074331.

Data Availability Statement: Some of the data used can be found in the references. Other data may be obtained from the authors upon reasonable request.

Conflicts of Interest: The authors declare no conflicts of interest

References

1. Horng, H.; Hong, C.; Yang, S.; Yang, H. Designing the refractive indices by using magnetic fluids. *Applied Physics Letters* **2003**, *82*, 2434–2436.
2. Martinez, L.; Cecelja, F.; Rakowski, R. A novel magneto-optic ferrofluid material for sensor applications. *Sensors and Actuators A: Physical* **2005**, *123*, 438–443.
3. Hong, C.; Yang, S.; Horng, H.; Yang, H.C. Control parameters for the tunable refractive index of magnetic fluid films. *Journal of Applied Physics* **2003**, *94*, 3849–3852.
4. Zegaar, I.; Hocini, A.; Harhouz, A.; Khedrouche, D.; Salah, H.B. Design of a double-mode Plasmonic wavelength filter using a defective circular nano-disk resonator coupled to two MIM waveguides. *Progress In Electromagnetics Research Letters* **2022**, *104*, 67–75.
5. Zu, P.; Chan, C.C.; Lew, W.S.; Jin, Y.; Liew, H.F.; Chen, L.H.; Wong, W.C.; Dong, X. High extinction ratio magneto-optical fiber modulator based on nanoparticle magnetic fluids. *IEEE Photonics Journal* **2012**, *4*, 1140–1146.
6. Dong, H.M.; Nga, L.T.Y.; Bang, N.H. Optical switching and bistability in a degenerated two-level atomic medium under an external magnetic field. *Applied Optics* **2019**, *58*, 4192–4199.

7. Li, Y.; Pu, S.; Hao, Z.; Yan, S.; Zhang, Y.; Lahoubi, M. Vector magnetic field sensor based on U-bent single-mode fiber and magnetic fluid. *Optics Express* **2021**, *29*, 5236–5246.
8. Knight, J.; Birks, T.; Russell, P.S.J.; Atkin, D. All-silica single-mode optical fiber with photonic crystal cladding. *Optics Letters* **1996**, *21*, 1547–1549.
9. De, M.; Singh, V.K. Magnetic fluid infiltrated dual core photonic crystal fiber based highly sensitive magnetic field sensor. *Optics & Laser Technology* **2018**, *106*, 61–68.
10. Li, J.; Wang, R.; Wang, J.; Zhang, B.; Xu, Z.; Wang, H. Novel magnetic field sensor based on magnetic fluids infiltrated dual-core photonic crystal fibers. *Optical Fiber Technology* **2014**, *20*, 100–105.
11. Liu, Q.; Li, S.; Wang, X. Sensing characteristics of a MF-filled photonic crystal fiber Sagnac interferometer for magnetic field detecting. *Sensors and Actuators B: Chemical* **2017**, *242*, 949–955.
12. Xu, J.; Gao, Y.; You, H. A Novel Structured Magnetic Field Sensor Based on Photonic Crystal Fiber Filled with Magnetic Fluid. *Crystals* **2022**, *12*, 1383.
13. Liu, S.; Li, S.; Yin, G.; Wang, X. Coupling characteristics of high birefringence dual-core As2S3 rectangular lattice photonic crystal fiber. *Chinese Physics B* **2012**, *21*, 034217.
14. Saitoh, K.; Koshiba, M. Numerical modeling of photonic crystal fibers. *Journal of Lightwave Technology* **2005**, *23*, 3580–3590.
15. Wang, Y.; Liao, C.; Wang, D. Femtosecond laser-assisted selective infiltration of microstructured optical fibers. *Optics Express* **2010**, *18*, 18056–18060.
16. Hunger, D.; Deutsch, C.; Barbour, R.J.; Warburton, R.J.; Reichel, J. Laser micro-fabrication of concave, low-roughness features in silica. *Aip Advances* **2012**, *2*, 012119.
17. Akowuah, E.; Gorman, T.; Ademgil, H.; Haxha, S. A highly sensitive photonic crystal fibre (PCF) surface plasmon resonance (SPR) sensor based on a bimetallic structure of gold and silver. 2012 IEEE 4th International conference on adaptive science & technology (ICAST). IEEE, 2012, pp. 121–125.
18. Chen, L.X.; Huang, X.G.; Zhu, J.H.; Li, G.C.; Lan, S. Fiber magnetic-field sensor based on nanoparticle magnetic fluid and Fresnel reflection. *Optics letters* **2011**, *36*, 2761–2763.
19. Saitoh, K.; Sato, Y.; Koshiba, M. Coupling characteristics of dual-core photonic crystal fiber couplers. *Optics Express* **2003**, *11*, 3188–3195.
20. Huang, W. Coupled-mode theory for optical waveguides: an overview. *JOSA A* **1994**, *11*, 963–983.
21. Eisenmann, M.; Weidel, E. Single-mode fused biconical coupler optimized for polarization beamsplitting. *Journal of Lightwave Technology* **1991**, *9*, 853–858.
22. Zhao, Y.; Wu, D.; Lv, R.; Li, J. Magnetic field measurement based on the Sagnac interferometer with a ferrofluid-filled high-birefringence photonic crystal fiber. *IEEE Transactions on Instrumentation and Measurement* **2016**, *65*, 1503–1507.
23. Zu, P.; Chan, C.C.; Lew, W.S.; Hu, L.; Jin, Y.; Liew, H.F.; Chen, L.H.; Wong, W.C.; Dong, X. Temperature-insensitive magnetic field sensor based on nanoparticle magnetic fluid and photonic crystal fiber. *IEEE Photonics Journal* **2012**, *4*, 491–498.
24. Dong, S.; Pu, S.; Huang, J. Magnetic field sensing based on magneto-volume variation of magnetic fluids investigated by air-gap Fabry-Pérot fiber interferometers. *Applied Physics Letters* **2013**, *103*, 111907.
25. Chen, Y.; Han, Q.; Liu, T.; Lan, X.; Xiao, H. Optical fiber magnetic field sensor based on single-mode–multimode–single-mode structure and magnetic fluid. *Optics Letters* **2013**, *38*, 3999–4001.
26. Dong, S.; Pu, S.; Wang, H. Magnetic field sensing based on magnetic-fluid-clad fiber-optic structure with taper-like and lateral-offset fusion splicing. *Optics Express* **2014**, *22*, 19108–19116.
27. Wei, F.; Mallik, A.K.; Liu, D.; Wu, Q.; Peng, G.; Farrell, G.; Semenova, Y. Magnetic field sensor based on a combination of a microfiber coupler covered with magnetic fluid and a Sagnac loop. *Scientific Reports* **2017**, *7*, 4725.
28. Liu, H.; Chen, C.; Wang, H.; Zhang, W. Simultaneous measurement of magnetic field and temperature based on surface plasmon resonance in twin-core photonic crystal fiber. *Optik* **2020**, *203*, 164007.